Chemistry & Biology
Article

Cholesterol *Seco*sterol Aldehydes Induce Amyloidogenesis and Dysfunction of Wild-Type Tumor Protein p53

Jorge Nieva,[1,5] Byeong-Doo Song,[2,3,6] Joseph K. Rogel,[2] David Kujawara,[2] Lawrence Altobel, III,[2,7] Alicia Izharrudin,[4] Grant E. Boldt,[4,8] Rajesh K. Grover,[2] Anita D. Wentworth,[2,9] and Paul Wentworth, Jr.[2,3,4,*]
[1]Department of Molecular and Experimental Medicine
[2]Department of Chemistry
[3]The Skaggs Institute for Chemical Biology
The Scripps Research Institute, 10550 N. Torrey Pines Road, La Jolla, CA 92037, USA
[4]Department of Biochemistry, University of Oxford, South Parks Road, Oxford OX1 3QU, UK
[5]Present address: Department of Oncology and Hematology, Billings Clinic, 2825 Eight Avenue N., P.O. Box 37000, Billings, MT 59107, USA
[6]Present address: Scripps Korea Antibody Institute, 192-1 Hyoja-dong, Chuncheon, Gangwon 200-701, Korea
[7]Present address: Anaptysbio, Inc., 10835 The Road to the Cure, San Diego, CA 92101, USA
[8]Present address: Bachem Americas, 3132 Kashiwa Street, Torrance, CA 90505, USA
[9]Present address: Prognosys Biosciences, Coast Boulevard South #310, La Jolla, CA 92037, USA
*Correspondence: paulw@scripps.edu
DOI 10.1016/j.chembiol.2011.02.018

SUMMARY

Epidemiologic and clinical evidence points to an increased risk for cancer when coupled with chronic inflammation. However, the molecular mechanisms that underpin this interrelationship remain largely unresolved. Herein we show that the inflammation-derived cholesterol 5,6-*seco*sterol aldehydes, atheronal-A (KA) and -B (ALD), but not the polyunsaturated fatty acid (PUFA)-derived aldehydes 4-hydroxynonenal (HNE) and 4-hydroxyhexenal (HHE), induce misfolding of wild-type p53 into an amyloidogenic form that binds thioflavin T and Congo red dyes but cannot bind to a consensus DNA sequence. Treatment of lung carcinoma cells with KA and ALD leads to a loss of function of extracted p53, as determined by the analysis of extracted nuclear protein and in activation of p21. Our results uncover a plausible chemical link between inflammation and cancer and expand the already pivotal role of p53 dysfunction and cancer risk.

INTRODUCTION

Inflammation, which functions at all three stages of tumor development (initiation, progression, and metastasis), is a host's response to acute tissue damage (Balkwill and Mantovani, 2001; Coussens and Werb, 2002; Lu et al., 2006). It is generally considered to play a role in tumor suppression by triggering an anti-tumor immune response (Philip et al., 2004) but can also stimulate tumor development (Balkwill and Mantovani, 2001; Philip et al., 2004). In this regard many chronic inflammatory conditions have associated neoplastic risk, e.g., the inflammatory bowel diseases, ulcerative colitis and Crohn's disease, are increased risk factors for colorectal carcinomas (Coussens and Werb, 2002). Similarly, chronic lung inflammation or infection has been associated with the development of lung cancer (Borm and Driscoll, 1996; Keeley and Rees, 1997). Basic research has shown that chronic inflammation appears to contribute to tumor progression by establishing a long-term milieu conducive to neoplasia (Coussens and Werb, 2002). However, the precise mechanisms by which inflammation achieves this remain to be determined.

The tumor suppressor protein p53 is a sequence-specific transcription factor that functions to maintain the integrity of the genome (Lane, 1992). On its induction/activation in response to DNA damage, p53 promotes cell-cycle arrest in G_1 phase (Kastan et al., 1991) and apoptosis if DNA repair is not possible. When p53 is inactivated, most commonly by a single missense mutation or by binding of viral oncoproteins to p53, cell growth can proceed without regulation, leading to tumor growth (Vogelstein and Kinzler, 1992). The critical nature of maintaining functional p53 within the cell is emphasized by the fact that mutations in the *P53* gene are detected in ~50% of human cancers (Hollstein et al., 1991) and that 90% of these mutations are in the core domain that is responsible for DNA binding (Hernandez-Boussard et al., 1999). In addition to mutant p53 being inactive, several types of malignant and premalignant tissues harbor a genetically wild-type but a transcriptionally inactive form of p53, often localized in their cytoplasm, hinting at epigenetic environmental triggers for p53 inactivation (Bosari et al., 1995; Isaacs et al., 1998; Moll et al., 1992, 1995; Tominaga et al., 1993).

Recently, we and others have discovered a process that is being studied in the context of a number of disease-related sporadic amyloidoses. We have shown that in vitro, certain inflammatory-derived lipidic aldehydes, when adducted to proamyloidogenic proteins in their native state, can induce misfolding and aggregation of native protein sequences (Wentworth et al., 2003; Zhang et al., 2004) (Figure 1). Thus, we have shown that the cholesterol 5,6-*seco*-sterols atheronal-A and -B (**KA**

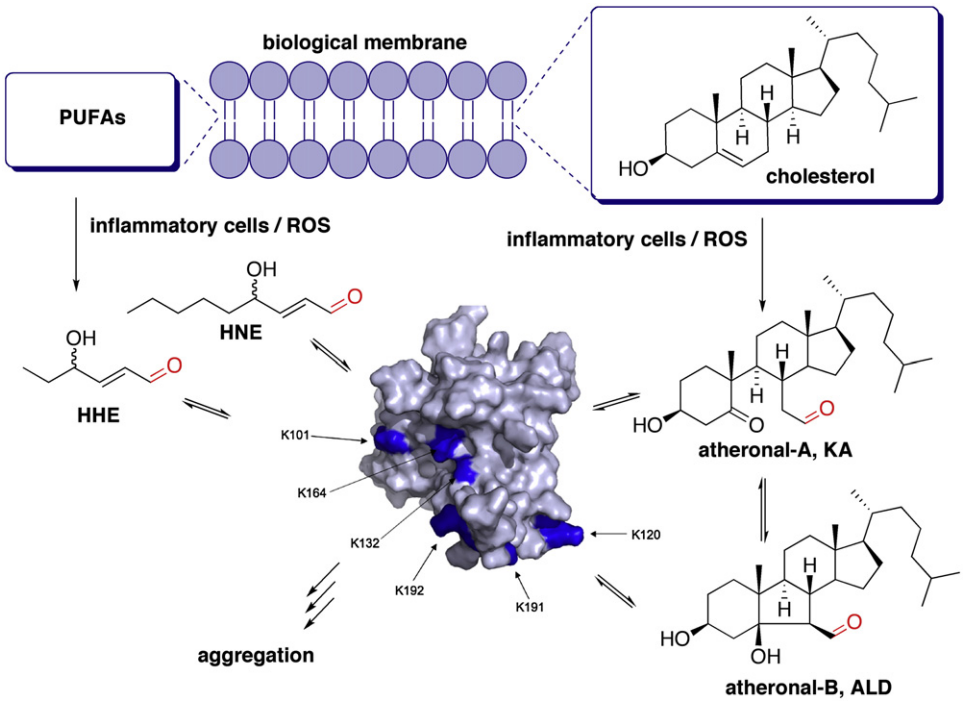

Figure 1. A Model for Lipid-Aldehyde Initiated p53 Inactivation

Scheme showing the concept of how membrane lipids, upon oxidation by reactive oxygen species (ROS), generate lipid-derived aldehydes such as **KA**, **ALD**, **HNE**, and **HHE**, which then adduct reversibly to lysine residues of cellular proteins, such as p53, which can then lead to misfolding/aggregation and dysfunction. The protein shown is a surface rendering of the p53 tetramerization domain (PDB reference 1tub), with surface lysines highlighted in blue.

and **ALD**, respectively), which are derived from oxidation of cholesterol by activated leukocytes during chronic inflammation, accelerate the in vitro misfolding of apoB$_{100}$, the protein component of low-density lipoprotein (LDL), under physiologically relevant conditions (Figure 1) (Wentworth et al., 2003). We and others have also shown that 4-hydroxynonenal (**HNE**; a major lipid peroxidation product of membrane lipids), **KA**, and **ALD** accelerate the in vitro amyloidogenesis of β-amyloid peptides (Aβ 1-40 and 1-42), leading to prefibrillar assemblies of Aβ (Zhang et al., 2004) via a process that involves a reversible site-specific modification of Aβ (Scheinost et al., 2008), and that **KA** and **ALD** accelerate the aggregation of α-synuclein (Bosco et al., 2006), leading to fibrillar aggregates. In addition we have shown that antibody light chains can be induced to aggregate by lipid aldehydes, both to form amyloid or amorphous aggregates, in a process dependant upon the specific aldehyde structure (Nieva et al., 2008). Most recently, we have shown that adduction of **KA** and **ALD** to a murine prion protein actually stabilizes the nonscrapie form of the prion and prevents/inhibits scrapie formation (Scheinost et al., 2009), showing that aldehyde adduction can be both proamyloidogenic and antiamyloidogenic, depending on which protein and which aldehyde are being studied.

Herein we report that the cholesterol-derived aldehydes **KA** and **ALD**, but not the polyunsaturated fatty acid (PUFA)-derived aldehydes **HNE** and 4-hydroxyhexenal (**HHE**), can induce amyloidogenesis of wild-type-p53 in a process that leads to a loss of function of p53. Given the known associations between inflammation and cancer, we see this as a potential new chemical link between the two syndromes, and it further highlights the potential for p53 misfolding, dysfunction, and cancer risk.

RESULTS AND DISCUSSION

Lipid-Derived Aldehydes Adduct to p53 and Induce Misfolding

Quiescent incubation of full-length recombinant wild-type hexahistidine-tagged human p53 (His$_6$-p53; 0.8 mg/ml) with the inflammatory aldehydes **KA**, **ALD**, **HNE**, and **HHE** (each at 100 μM) in phosphate-buffered saline (PBS) (pH 7.4) with ethanol (0.1% v/v) as a cosolvent leads to the acceleration in formation of thioflavin-T (ThT)-positive aggregates with the cholesterol *seco*-sterol aldehydes (time to half-maximal fluorescence: **KA**, t_{50} ~80 min; **ALD**, t_{50} ~100 min), but not with the α,β-unsaturated inflammatory aldehydes **HHE** and **HNE**, relative to vehicle (**VEH**; PBS [pH 7.4], containing 0.1% v/v ethanol) (Figure 2A). The fluorescence emission of the dye ThT is increased upon binding to protein aggregates with a cross-β sheet structure (LeVine, 1999), either fibrillar or nonfibrillar in morphology (Hurshman et al., 2004; Zhang et al., 2004). The time course of ThT fluorescence observed for the **KA** and **ALD**-initiated His$_6$-p53 amyloid formation, a rapid rise in ThT fluorescence to a plateau phase with no lag phase, is indicative of a "seeded" or so-called downhill polymerization that is thermodynamically favored from the outset (Ferrone, 1999), and is in line with what we have observed previously for the atheronal-initiated polymerization of β-amyloid and α-synuclein (Bosco et al., 2006; Zhang et al., 2004).

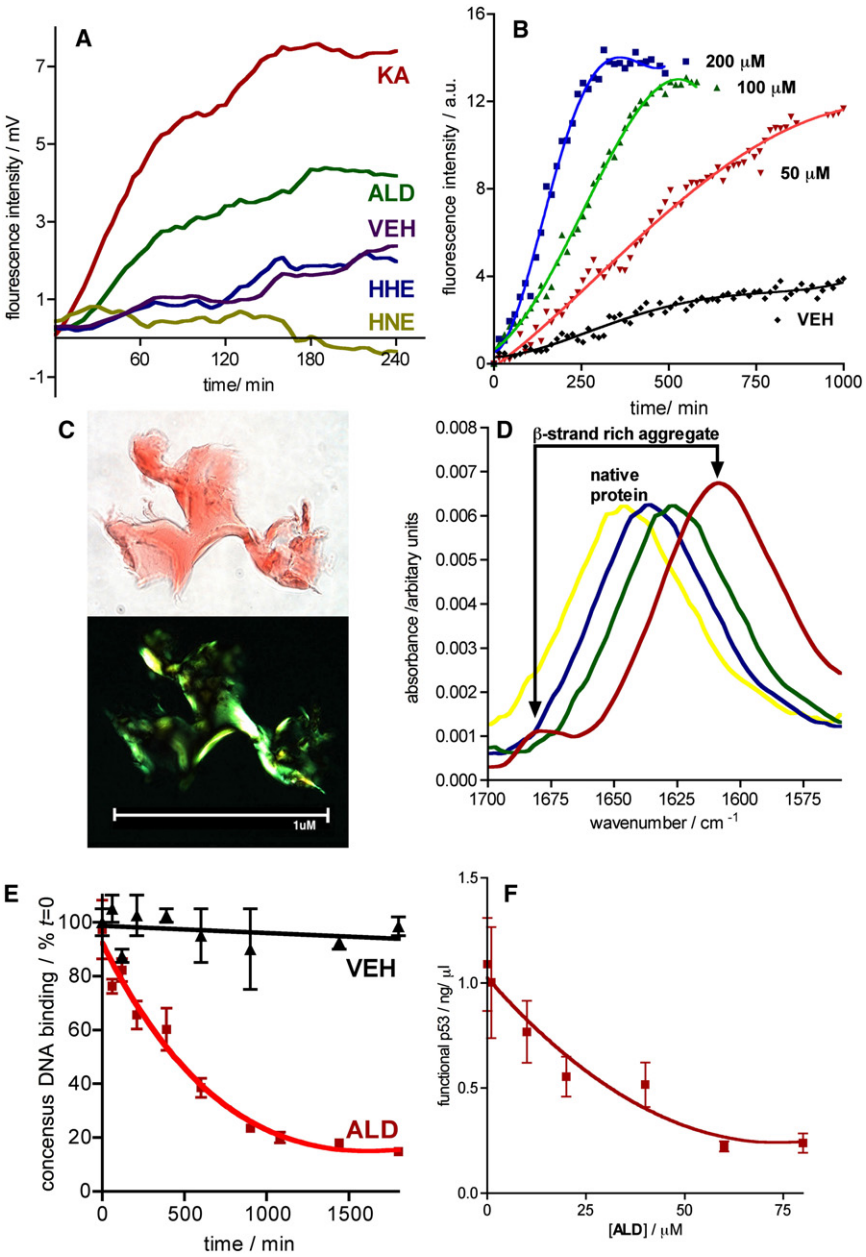

Figure 2. Lipid Aldehydes KA and ALD, but Not HNE and HHE, Induce Amyloidogenesis and Dysfunction of Recombinant His_6-p53

(A) Graph of ThT fluorescence versus time during quiescent incubation of His_6-p53 (0.8 mg/ml) in PBS (pH 7.4) with ethanol (0.1% v/v) cosolvent in the presence of **KA**, **ALD**, **HNE**, or **HHE** (each at 100 μM). Data are reported as the mean fluorescence emission (excitation, 440 nm; emission, 485 nm) of duplicate experiments.

(B) Graph of **KA** concentration-dependent (0–200 μM) quiescent aggregation of His_6-p53 (0.8 mg/ml) in PBS (pH 7.4) with ethanol (0.1% v/v) cosolvent, as measured by ThT fluorescence. Data are reported as the mean fluorescence (excitation, 440 nm; emission, 485 nm) of duplicate experiments. Data are fitted to a third-order polynomial using GraphPad Prism 4 for Macintosh.

(C) Optical microscope images (100×) obtained under normal (upper) and cross-polarized (lower) light of aggregates generated by incubation of His_6-p53 (0.8 mg/ml) with **KA** (25 μM) for 5 hr, followed by centrifugation and staining with Congo red (100 μM).

(D) FTIR spectra at times (0 min [yellow], 300 min [blue], 800 min [green], and 1200 min [(red]) during the quiescent aggregation of His_6-p53 (0.5 mg/ml) in D_2O with **KA** (100 μM).

(E) Graph of functional p53 (as a percentage of t = 0) versus time during the quiescent aggregation of His_6-p53 (0.8 mg/ml) in the presence of **ALD** (50 μM) or **VEH** (ethanol 0.1% v/v). Data are mean ± SEM of at least duplicate determinations. Data for **VEH** are fitted to a linear regression analysis (r^2 = 0.992); data for **ALD** are fitted to a single-phase exponential decay using GraphPad Prism 4.

(F) Graph of functional p53 (in ng/ml) versus **ALD** during a 2 hr quiescent aggregation of His_6-p53 (0.8 mg/ml) in the presence of **ALD** (0–80 μM). Data are reported as the mean ± SEM of at least duplicate determinations. Data are fitted to a single-phase exponential decay using GraphPad Prism 4.

See also Figure S1.

Atheronal-Induced Misfolding of p53 Leads to Amyloid Aggregates

The atheronal-induced aggregation of His_6-p53 was studied in some detail and is concentration dependent, exhibiting an increase in the initial rate of ThT fluorescence as the ratio of **KA** to p53 increases (Figure 2B). In addition the plateau phase appears to be independent of **ALD** concentration but is reached faster at higher concentrations of lipid aldehyde. Incubation of His_6-p53 with **KA** generates aggregates that exhibit classic apple-green birefringence under polarizing light, when stained with Congo red dye, further strengthening the notion that incubation with cholesterol *seco*-sterols generates amyloid fibrillar p53 aggregates (Figure 2C). In addition TEM analysis of His_6-p53 incubated with **ALD** reveals ribbon-like unbranched fibrillar assemblies (see Figure S1 available online).

To gain insight into the structural transition from native wild-type His_6-p53 to its **KA**-induced misfolded state, we recorded FT-IR spectra during the incubation of His_6-p53 with **KA** (Figure 2D). In the absence of **KA**, the FT-IR of the native structure of His_6-p53 is unchanged. However, the FT-IR spectrum of His_6-p53 during incubation with **KA** (100 μM) at 37°C in PBS (pH 7.4) exhibits a time-dependant shift of the amide-I absorbance band (t = 0 min, λ_{max}^{-1} = 1647 cm^{-1}; t = 300 min, λ_{max}^{-1} = 1635 cm^{-1}; t = 800 min, λ_{max}^{-1} = 1626 cm^{-1}; t = 1200 min, λ_{max}^{-1} = 1609 cm^{-1}). Thus, the FT-IR spectrum of His_6-p53 at t = 0 and 37°C in PBS is dominated by a strong absorbance at 1647 cm^{-1}, corresponding to α helices. As quiescent

incubation with **KA** progresses, this absorbance band shifts to lower wave numbers, consistent with unfolding of α helices and increased random peptide conformations. After incubation for 1200 min, the absorbance is increased and is centered at 1609 cm^{-1}, characteristic of β strands in amyloid fibrils. There is also an accompanying weaker absorbance band at 1683 cm^{-1}, also indicative of β strand containing structures with strong intermolecular hydrogen bonds, classic evidence of amyloid formation.

The process by which amyloid fibrillization occurs from natively folded proteins is constrained by aggregation from partially unfolded intermediates (Uversky and Fink, 2004). Therefore, proteins such as p53 require partial unfolding prior to the onset of fibril formation. To explain the molecular basis of amyloid fibril formation, it has been proposed that fibrillization can occur when the rigid native structure of a protein is destabilized, favoring partial unfolding and culminating in formation of a partially unfolded conformation or intermediate (Dobson, 1999; Kelly, 1998). In the context of p53, very few studies have been performed on the full-length protein; however, a number of biophysical studies of the p53 tetramerization domain have revealed that at acidic pH (4.0) and 37°C, a mutant tetramerization domain p53tet-R337H forms fibrils much faster than p53-tetwt, as monitored by ThT fluorescence. Interestingly, the time-dependent profiles of ThT fluorescence p53tet-R33H incubated at pH 4.0 and **KA**-treated His_6-p53 are remarkably similar. Specifically, there is no apparent lag phase in the aggregation, with peak ThT fluorescence occurring between 2 and 4 hr. Therefore, the rationale proposed for the atheronal-induced aggregation of p53 in our work is in line with what has been proposed for p53-tet-R337H, which involves partial unfolding followed by assembly into proamyloid oligomers and fibrillization.

Atheronal-Misfolded p53 Cannot Bind to DNA

To investigate whether atheronal treatment of His_6-p53 leads to a loss of DNA binding, we utilized an ELISA that detects p53 when bound to a consensus duplex deoxyoligonucleotide sequence. Thus, the ELISA is a primary readout of DNA-bound p53 and does not detect p53 that is not bound to DNA. Quiescent incubation of His_6-p53 (0.8 mg/ml) with **ALD** (50 μM) in PBS (pH 7.4) leads to a time-dependant loss of DNA binding (Figure 2E). Thus, incubation of His_6-p53 for 30 hr with **ALD** (50 μM) leads to an ~85% drop in DNA-binding ability of p53, as determined by ELISA, whereas incubation with **VEH**, under the same conditions, leads to a drop of <10% in DNA binding. The impact of atheronal incubation on His_6-p53 function is also concentration dependent. Incubation of His_6-p53 (0.8 mg/ml) for 24 hr with **ALD** (0–80 μM) leads to increased reduction in p53-DNA binding (Figure 2F).

Interestingly, a comparison of the time-dependent changes induced by incubation of His_6-p53 with **ALD** on ThT fluorescence and DNA binding reveals that the ThT fluorescence plateau is reached at ~240 min (Figure 2A), whereas the maximum impact on DNA binding is not reached until ~1300 min (Figure 2E). Although the reasons for this disparity are unresolved, what is clear is that ThT fluorescence is a precise measure of amyloid structural changes, whereas the ELISA is a readout for any structural change, amyloid and nonamyloid, that impairs DNA binding. Therefore, an explanation of the two sets of data, ThT-fluorescence and DNA binding, is that **ALD** induces amyloid changes in p53 structure first, followed by, or in concert with, longer duration nonamyloid-like changes in p53, and it is the nonamyloid changes that impact p53 DNA binding. This explanation of amyloid and nonamyloid changes in His_6-p53 induced by **ALD** is supported by the fact that the solution turbidity of **ALD**-treated p53, under conditions in Figure 2A, is visibly increased after 24 hr, whereas at 4 hr (where ThT fluorescence has reached a plateau), the solution is not visibly turbid.

Lipid-Derived Aldehydes Induce Misfolding of p53 in Cultured Cells

To investigate the effect of lipid aldehydes on p53 in a cell-based system, we treated the lung carcinoma cell line A-427, known to upregulate wild-type p53 during UV or radiation-based stress. Thus, cultured A-427 cells were exposed to γ-irradiation (5000 cGy) and then media were replaced with **KA**, **ALD**, **HNE**, **HHE** (each at 20 μM), or **VEH** in media with 0.1% ethanol (cosolvent). The cells were then incubated at 37°C for a further 24 hr. After incubation of the cells with aldehydes, nuclear protein was extracted, and the DNA binding of p53 was assessed by ELISA as described vide supra (Figure 3A). The levels of p53 extracted from all treated cells were essentially unchanged; however, the DNA-binding ability of p53 levels was significantly different in all aldehyde-treated cells ($p < 0.05$), relative to **VEH**. **HHE**-treated cells had an elevated level of functional p53 relative to **VEH** (1.6 × **VEH**; $p < 0.05$), and while the mechanism by which this effect is under investigation, this may be due to a redistribution of functional p53 from the cytosol to the nucleus. **HNE**-treated cells have a significantly reduced level of DNA-binding nuclear p53 relative to **VEH** (33% of **VEH**; $p < 0.05$), and given that **HNE** does not induce p53 misfolding (Figure 2A), this hints at an indirect off-target mechanism by which **HNE** is causing p53 dysfunction. Previous work by Moos and coworkers (Cassidy et al., 2006) has shown that certain endogenous αβ-unsaturated prostaglandin-derived aldehydes, such as PGA_1 and PGA_2, can cause p53 misfolding in cells, by a process that involves the chemical modification and inactivation of the selenoprotein, thioredoxin reductase (TrxR) (Moos et al., 2000, 2003). Therefore, it seems plausible that **HNE**, which is an αβ-unsaturated aldehyde and is known to inactivate TrxR (Cassidy et al., 2006), is inducing p53 dysfunction indirectly via this mechanism.

The most dramatic disruption of p53 DNA binding in nuclear extracts of A-427 cells occurs after incubation with the cholesterol *seco*-sterols, **KA** and **ALD** (Figure 3A). There is very little DNA binding of p53 in nuclear extracts from A-427 incubated with **KA** and **ALD** (3.4%, $p < 0.05$ and 4.2%, $p < 0.05$ of **VEH**, respectively). Extrapolation of the misfolding studies in Figure 2 to this p53 extraction data is complicated by potential off-target effects in cells; however, it seems clear that the atheronals that induce direct misfolding of p53 are far more impactful on a mole for mole equivalence at disrupting functional p53 in cells than **HNE** and **HHE** that have no direct effect on p53 misfolding. Thus, whereas there may be indirect, off-target processes by which certain aldehydes, such as **HNE**, PGA_1, and PGA_2, influence p53 function, the direct induction of p53 misfolding is a potent mechanism by which inflammatory aldehydes can modulate p53 binding to DNA.

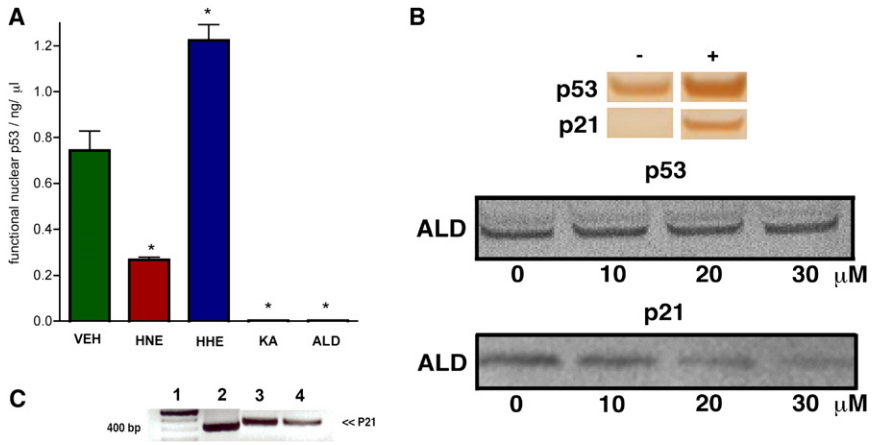

Figure 3. Lipid Aldehydes Affect Wild-Type p53 DNA Binding and p21 Activation in Cells

(A) Bar chart representing level of DNA binding nuclear p53 extracted from A-427 cells incubated at 37°C for 24 hr with **VEH** (0.1% ethanol), **HNE**, **HHE**, **KA**, or **ALD** (each at 40 μM) after receiving a dose of γ-radiation (5000 cGy). After the incubation, nuclear extracts were taken, and total protein (BCA), p53 (western blot), and functional p53 (ELISA) were measured. Data are reported as the mean ± SEM of triplicate determinations. Data were analyzed using a Student's two-tail t test and were considered significantly different from **VEH** (*) if $p < 0.05$.

(B) Upper view is a western blot analysis of p53 and p21 in nuclear protein extracts from A-427 cells before (−) and after (+) receiving γ-radiation (5000 cGy). Lower view is a western blot analysis of p53 and p21 in nuclear protein extracts from A-427 cells. Cells were incubated at 37°C for 24 hr with **ALD** (0–30 μM) after receiving a dose of γ-radiation (5000 cGy). After the incubation, nuclear extracts were taken, and total protein (BCA), p53, and p21 (western blot) were measured.

(C) Agarose gel analysis of p21 PCR DNA derived from p53 immunoprecipitation (IP) of A-427 genomic DNA. Lane 1 shows 100 bp ladder; lane 2, A-427 genomic DNA with p53 IP (after irradiation); lane 3, A-427 genomic DNA with p53 IP (after irradiation and incubated with **VEH** for 20 hr); and lane 4, A-427 genomic DNA with p53 IP (after irradiation, **ALD,** 30 μM for 20 hr).

Atheronals Impair p53 Chromatin Binding and p53-Mediated Transcription

Genome damage usually increases the cellular levels of wild-type p53 tumor suppressor and p53-dependent transcription (Lane, 1992; Levine et al., 1991; Vogelstein and Kinzler, 1992; Zambetti and Levine, 1993). Consistent with this phenomenon, exposure of A-427 cells to γ-irradiation (5000 cGy) leads to a proportional increase in p53 protein and its transcriptionally regulated protein, p21, relative to untreated cells (Figure 3B, upper). Western blot analysis of p53 and p21 extracted from A-427 cells that had been exposed to γ-irradiation (5000 cGy) and subsequently incubated with **ALD** (0–30 μM) reveals that nuclear p53 levels remain unchanged with increasing levels of atheronals (Figure 3B, middle). However, **ALD** treatment of A-427 cells causes an atheronal concentration-dependent reduction in the expression of p21 (Figure 3B, lower). This atheronal-induced reduction in p21 expression is supported by chromatin immunoprecipitation (ChIP) studies from atheronal-treated A-427 cells. Purification of sheared chromatin, immunoprecipitated by an anti-p53 antibody, followed by PCR of the purified chromatin fragments, with p21 primers (forward 5′-CC AGCCCTTGGATGGTTT-3′; reverse 5′-GCCTCCTTTCTGTGCC TGA-3′) reveals that atheronal treatment leads to a reduction in p21 expression (Figure 3C). These combined data suggest that the atheronals do not directly impact the nuclear level of p53 but by inducing p53 misfolding, may cause a direct reduction in p53 transactivation within the cell.

For the aldehydes KA and ALD to impact p53 misfolding in the cells, they must come into direct contact with the protein and to do this, have to either enter the nucleus or cytoplasm because p53 exists in equilibrium between the nucleus and cytoplasm. Although we have yet to perform an in-depth study of the trafficking of the atheronals in cells, what we have shown previously is that a fluorescently tagged **ALD** analog is rapidly taken up (within 5 min) into cultured macrophages (J774), by a process of diffusion, and traffics to all compartments of the cell, excluding the nucleus (Takeuchi et al., 2006). Therefore, the cellular effects we observe on the A-427 cell line here are most likely initiated by interaction between ALD and p53 in the cytoplasm, which then in its misfolded form is either sequestered in the cytoplasm, preventing its movement into the nucleus, or moves into the nucleus where it is unable to bind to DNA.

The concentration of **ALD** that we show achieves clear DNA-binding reduction in A-427 cells is ~20 μM (Figure 2F). The concentration of *seco*sterols in the systemic circulation is ~30 nM, whereas patients with inflammatory artery disease have almost a log higher level of circulating aldehyde (~200 nM) (Wentworth et al., 2003). However, what is not yet known are the effective local concentrations of atheronals in tissues that are undergoing a chronic inflammatory response, as would be the case in tumorigenic systems, which may be much higher than in systemic circulation. An example of such a difference is observed with **HNE**, which has nanomolar circulating concentrations but cell membrane levels as high as millimolar (Esterbauer, 1982; Esterbauer et al., 1990, 1991). Therefore, the concentrations of ALD required to reduce p53 binding in cells are not beyond the plausible levels achievable under the pathological syndrome being studied.

We propose that endogenous lipid-derived aldehydes are able to adduct to surface-exposed lysine residues on wild-type p53 protein, and in doing so specific aldehydes, such as the cholesterol *seco*-sterol aldehydes (**KA** and **ALD)**, but not the PUFA-derived α,β-unsaturated aldehydes (**HNE** and **HHE**), can induce a direct misfolding p53 event that is amyloidogenic. This **KA** and **ALD**-induced misfolding event renders the p53 unable to bind to DNA in vitro, and exposure of cultured lung carcinoma cells to the atheronals leads to a dramatic ($p < 0.05$) reduction in the amount of DNA-binding nuclear p53 protein (but not total nuclear p53) and a reduction in transactivation of p21.

Finally, the observation that only certain aldehydes induce the misfolding of p53 suggests that there is a molecular recognition aspect to the aggregation process. This observation of molecular recognition between an aggregation-prone protein and the

atheronal aldehydes has also been observed with lipid aldehyde-initiated aggregation of β-amyloid peptides (Scheinost et al., 2008). The importance of the recognition of the lipid's structure to protein aggregation is that this noncovalent recognition should be able to be mimicked, leading to the development of molecular chaperones that will protect p53 from the aldehyde-initiated protein misfolding event and lead to potential new anticancer drugs.

SIGNIFICANCE

What we show, to our knowledge, for the first time is that direct modification of p53 by certain endogenous aldehydes is sufficient to cause structural changes in p53 that may contribute to epigenetic silencing. This direct inactivation of p53 by cholesterol-derived aldehydes may be a hitherto unknown chemical link between inflammation and cancer, and may contribute in part to the known cancers where wild-type inactivation of p53 has been reported, such as breast cancer (Moll et al., 1992), neuroblastoma (Isaacs et al., 1998; Moll et al., 1995), colon adenocarcinoma (Bosari et al., 1995), and colon adenoma (Tominaga et al., 1993).

EXPERIMENTAL PROCEDURES

Cells and Proteins

The human A-427 lung carcinoma cell line carries wild-type p53. The recombinant His_6-p53 was purified from *E. coli* BL21 (DE3) transformed with pET-15b plasmid containing the open reading frame for p53.

Recombinant His_6-p53 Expression, Purification, and Refolding

The open reading frame encoding wild-type p53 was cloned by PCR into pET-15b (Novagen) between NdeI and BamHI sites. PCR was performed on pCMV-XL5-p53 from OriGene (Rockville, MD) using two primers: 5′-GAG AGA CAT ATG GAG GAG CCG CAG TCA GAT CC-3′, and 5′-GAG AGA GGA TCC TCA TCA GTC TGA GTC AGG CCC TTC TG-3′. The resulting plasmid, pET-15b-p53, was transformed into *E. coli* BL21 (DE3) (Invitrogen) for expression. The overnight culture from a single colony was diluted 1:100 into 1 liter of Luria Bertani media containing 100 mg/ml ampicillin, which then was incubated with shaking at 37°C until an OD_{600} of 0.6–0.8. Recombinant protein expression was induced overnight at OD_{600nm} of 0.4 by addition of 0.5 mM isopropyl-β-D-thiogalactopyranoside (IPTG) at 25°C. After centrifugation at 5000 rpm for 15 min, the cell pellets (2–4g) were frozen overnight at −20°C.

More than 70% of the recombinant protein, expressed as detailed above, deposits into inclusion bodies, and isolation was carried out after bacterial cell lysis using 5 ml of BugBuster (Novagen) per gram of wet pellet, benzonase nuclease, and EDTA-free protease inhibitors, followed by centrifugation at 5000 × g for 30 min. The inclusion bodies were washed again with 10% BugBuster to further remove cell debris and other proteins. For solubilization the inclusion bodies were resuspended in 1 ml of 100 mM Tris-HCl, 6 M Guanidinium Chloride (GdmCl), 50 mM DTT at pH 8.0. Renaturation of the recombinant proteins isolated from the inclusion bodies was performed in refolding buffer consisting of 50 mM sodium phosphate, 1 M L-arginine, 2 mM DTT, 0.2 mM $ZnCl_2$ at pH 8.0. The samples were incubated for 10 hr at 4°C. For large-scale production (200 ml refolding buffer), pulse renaturation of p53 was followed (solubilizate was added to the renaturation buffer six times with approximately 150 μg/ml per step and an interval of 90 min between each addition). After an overnight dialysis against 50 mM NaPPhos, 5% (v/v) glycerol, 4 mM DTT, pH 8.0 at 4°C, the renatured proteins were precipitated using 30,000 MWCO Vivaspin centricons (Sartorius).

Refolded protein samples were applied to the QIAGEN Ni-NTA Fast Start 2 ml purification columns. All fractions were collected and were analyzed with 10% SDS-PAGE and western blot using a murine monoclonal antibody for p53 (Abcam; catalog number ab1101).

ThT Binding and Fluorescence of His_6-p53 with Lipid Aldehydes

Recombinant His_6-p53 (0.8 mg/ml) was incubated in at least duplicate with lipid aldehydes **KA**, **ALD**, **HNE**, **HHE** (final concentration 100 μM), or **VEH** in PBS (pH 7.4), and ethanol (0.1% v/v cosolvent) at 37°C and in the presence of Th-T (10 μM) in a 384-well microtiter plate (final assay volume 50 ml). Time-dependent changes in the fluorescence (excitation, 440 nm; emission, 485 nm) of the assays were measured on a SpectraMax Gemini XS fluorescence detector (Molecular Devices, Union City, CA). Please note that all the noncell-based assays reported in this study were performed with the His_6-p53 recombinant protein. However, we have performed ThT aggregation assays with human wild-type p53 (Calbiochem, San Diego CA) and **KA**, and the time course of fluorescence, both with **VEH** and **KA** (100 μM), was identical to the wild-type p53 that we observed with our recombinant His_6-p53 protein construct. In addition, please note that for ease of assay, the ThT was present during the aggregation assay. However, we have performed ThT aggregation assays where assay aliquots are removed and added to a ThT solution (10 μM) in PBS (pH 7.4), both with **VEH** and **KA** (100 μM), and the profiles were identical to that we observed with ThT in the aggregation assay. Also note incubation of ThT with **VEH**, **KA**, **ALD**, **HNE**, or **HHE** had no measurable effect on ThT fluorescence excitation or emission.

Congo Red Binding and Birefringence

Wild-type native His_6-p53 (0.7 mg/ml), prepared and purified as detailed above, was incubated with **KA** (25 μM) in PBS (pH 8.0) with ethanol (4.0% v/v) for 5 hr at room temperature (assay volume 100 μl) in a protein concentration tube (Millipore). Congo red (100 μM in 1% ethanol in water) was added, and the mixture was allowed to stand at room temperature for 30 min. The resultant sample was then centrifuged (Millipore) at 3600 rpm for 30 min. The concentrated supernatant and aggregates were then added to a glass slide and warmed at 37°C for 10 min. Glycerol and a coverslip were then applied. Aggregates were analyzed under normal and phase-contrast light microscopy conditions (100× magnification; Olympus BX51 microscope). Images were recorded on an Olympus MicroFire camera.

FTIR Studies

In a typical experiment, His_6-p53 (0.5 mg/ml) in refolding buffer, prepared as detailed above, was dialyzed overnight in deuterium oxide at 4°C. Prior to FTIR experiments, the binding activity of the His_6-p53 was tested using the ELISA-based TransBinding assay kit (Panomics, Redwood City, CA) detailed below.

The misfolding process was started by addition of **KA** (100 μM final concentration) or **VEH** to the solution of His_6-p53 (0.5 mg/ml) in D_2O with incubation at room temperature. FTIR spectra were recorded throughout the assay at room temperature on a Bio-Rad FTS 6000 FTIR machine, equipped with diamond-attenuated total reflectance (ATR) with a He-Ne laser detector. Each spectrum was the average of 100 spectra recorded over the course of 100 min. The raw absorbance data were exported into Microsoft Excel and GraphPad Prism 4 for Macintosh for analysis.

Effect of ALD on DNA Binding of His_6-p53

Wild-type His_6-p53 protein (final concentration 0.8 mg/ml), prepared as described above, was incubated in at least duplicate with lipid aldehyde **ALD** (final concentration of 50 μM) or **VEH** in PBS (pH 7.4) and ethanol (0.1% v/v cosolvent) at 37°C. At times during the incubation, aliquots were removed, and DNA binding was measured by the Panomics ELISA TransBinding kit. Data are reported as the mean ± SEM of the functional p53 as a percentage (%) of t = 0. Data analysis was performed using GraphPad Prism 4 for Macintosh.

Recombinant wild-type His_6-p53 protein (final concentration of 0.8 mg/ml), prepared as described above, was incubated in at least duplicate with lipid aldehyde **ALD** at various concentrations (0–80 μM) in PBS (pH 7.4), and ethanol (0.1% v/v cosolvent) at 37°C. After 2 hr of incubation, DNA binding of the p53 was measured by the Panomics ELISA described above. Data are reported as the mean ± SEM of the functional p53 as nanogram per milliliter. Data analysis was performed using GraphPad Prism 4 for Macintosh.

Incubation of A-427 Cells with Lipid Aldehydes

Human lung carcinoma (ATCC; #HTB-53, A-427) cells were routinely cultured in fetal calf serum (FCS; 10%) with minimum essential medium (MEM) and

L-glutamine (2 mM), sodium bicarbonate (1.5 g/l), nonessential amino acids (0.1 mM), and sodium pyruvate (1 mM) to 80%–90% confluency in 75 cm^2 flasks. A-427 cells were then exposed to γ-irradiation (5000 cGy) from a cesium source, media were replaced, and the cells were incubated for 24 hr in growth medium. At this time, media were replaced with fresh media (15 ml) containing **KA**, **ALD**, **HNE**, **HHE** (each at 40 μM), or **VEH** (ethanol, 0.1% v/v) in at least duplicate and incubated for a further 24 hr at 37°C. The cells were then pelleted by centrifugation and washed with PBS (pH 7.4). Nuclear extracts were obtained using a nuclear extraction kit (Panomics). Protein concentration of the extracts was determined using a BCA protein assay kit (Pierce, Rockford, IL), and p53 concentration was measured using western blot analysis. Quantification of functional p53 was assessed by DNA binding using the Panomics TransBinding p53 assay kit as detailed above. Five and 2.5 μg of nuclear extract were added per well of the ELISA in duplicate for each condition, respectively. The data for functional p53 (reported as mean ± SEM) were determined by taking the raw absorbance data and interpolating from a standard curve of known concentrations of wild-type p53 using GraphPad Prism 4 for Macintosh.

ALD Treatment of A-427 Cells

A-427 cells were exposed to γ-irradiation (5000 cGy) from a cesium source, media were replaced, and the cells were incubated for 24 hr in growth medium. At this time, media were replaced with fresh media (15 ml) containing **ALD** (40 μM) and **VEH** (ethanol, 0.1% v/v) in at least duplicate and incubated for varying times up to 30 hr at 37°C. At various times throughput the incubation, cells were pelleted by centrifugation and washed with PBS (pH 7.4). Nuclear extracts were obtained using a nuclear extraction kit (Panomics). Protein concentration of the extracts was determined using a BCA protein assay kit (Pierce), and p53 concentration was measured using western blot analysis. Quantification of functional p53 was assessed by DNA binding using the Panomics TransBinding p53 assay kit as detailed above. Nuclear extract (5 and 2.5 μg) was added per well of the ELISA in duplicate for each condition, respectively. The data for functional p53 (reported as mean ± SEM) were determined by taking the raw absorbance data and interpolating from a standard curve of known concentrations of wild-type p53 using GraphPad Prism 4 for Macintosh.

Measurement of p21 WAF Transcription

A-427 human lung carcinoma (ATCC; #HTB-53) cells were grown in FCS (10%) MEM with L-glutamine (2 mM), sodium bicarbonate (1.5 g/l), nonessential amino acids (0.1 mM), and sodium pyruvate (1 mM) to 80%–90% confluency in 75 cm^2 flasks. The cells were exposed to γ-irradiation (5000 cGy) from a cesium source, media were replaced, and the cells were incubated for 24 hr with **VEH** (0.1% ethanol) or **ALD** at 10–30 μM in at least duplicate. The cells were then incubated for a further 16 hr. Nuclear extracts were obtained from each condition using the Panomics Nuclear Extraction Kit (catalog number AY2002). Protein concentration was determined for each extract using the Pierce BCA protein assay kit (catalog number 23225). The nuclear extracts were frozen at −80°C and then analyzed by western blots. The PVDF membranes were developed using the WesternBreeze Chromogenic Immunodetection Kit (Invitrogen; catalog number WB7103). Total protein was visualized with Ponceu S solution (Sigma-Aldrich; catalog number P-7170). The primary antibodies, mouse anti-human p53 (BD; catalog number 554167) and mouse anti-human p21 (BD; catalog number 554262), were diluted 1:500 and incubated overnight.

p21 ChIP Assay Protocol

A-427 cells were cultured to 80% confluence as detailed above. The cells were exposed to γ-irradiation (5000 cGy) from a cesium source, media were replaced, and the cells were incubated for 20 hr with **VEH** (0.1% ethanol) or **ALD** at 30 μM in at least duplicate. Cells were harvested by trypsinization, counted, and lysed using standard protocols. For chromatin shearing, cell lysates were sonicated with a Misonix 3000 ultrasonicating bath at 4°C (270 W, 20 cycles: 30 s pulse with 2 min cooling). A 1 kb DNA smear confirmed successful shearing. For p53 immunoprecipitation, sheared lysates were diluted 2:1 with antibody dilution buffer. A total of 5 μg/sample of biotinylated goat anti-human p53 antibody was then added; please note that biotinylated goat anti-IgG was added as a negative control. Samples were then incubated for 17 hr at 4°C, with shaking at 250 rpm. Streptavidin agarose was then added to the immunoprecipitation mixture, and the mixture was incubated for 30 min at 4°C with shaking, followed by addition of chelating resin and elution. For purification and PCR of immunoprecipitated DNA, the immunoprecipitated DNA was purified using QIAquick PCR Purification Kit (#28106), and PCR was performed using p21 primers.

SUPPLEMENTAL INFORMATION

Supplemental Information includes one figure and can be found with this article online at doi:10.1016/j.chembiol.2011.02.018.

ACKNOWLEDGMENTS

P.W. would like to thank all members of the Wentworth groups, in Oxford and La Jolla, their support. This work was supported by the NIH (AG028300), the ALSAM foundation (J.N.), and the Skaggs Institute for Research (P.W.), and a grant from The Scripps Research Institute (P.W.).

Received: November 21, 2009
Revised: January 24, 2011
Accepted: February 15, 2011
Published: July 28, 2011

REFERENCES

Balkwill, F., and Mantovani, A. (2001). Inflammation and cancer: back to Virchow? Lancet *357*, 539–545.

Borm, P.J., and Driscoll, K. (1996). Particles, inflammation and respiratory tract carcinogenesis. Toxicol. Lett. *88*, 109–113.

Bosari, S., Viale, G., Roncalli, M., Graziani, D., Borsani, G., Lee, A.K., and Coggi, G. (1995). p53 gene mutations, p53 protein accumulation and compartmentalization in colorectal adenocarcinoma. Am. J. Pathol. *147*, 790–798.

Bosco, D.A., Fowler, D.M., Zhang, Q., Nieva, J., Powers, E.T., Wentworth, P., Jr., Lerner, R.A., and Kelly, J.W. (2006). Elevated levels of oxidized cholesterol metabolites in Lewy body disease brains accelerate alpha-synuclein fibrilization. Nat. Chem. Biol. *2*, 249–253.

Cassidy, P.B., Edes, K., Nelson, C.C., Parsawar, K., Fitzpatrick, F.A., and Moos, P.J. (2006). Thioredoxin reductase is required for the inactivation of tumor suppressor p53 and for apoptosis induced by endogenous electrophiles. Carcinogenesis *27*, 2538–2549.

Coussens, L.M., and Werb, Z. (2002). Inflammation and cancer. Nature *420*, 860–867.

Dobson, C.M. (1999). Protein misfolding, evolution and disease. Trends Biochem. Sci. *24*, 329–332.

Esterbauer, H. (1982). Aldehydic products of lipid peroxidation. In Free Radicals, Lipid Peroxidation and Cancer, D.C.H. McBrien and T.F. Slater, eds. (London: Academic Press), pp. 101–128.

Esterbauer, H., Zollner, H., and Schaur, R.J. (1990). Aldehydes formed by lipid peroxidation: mechanisms of formation, occurrence, and determination. In Membrane Lipid Oxidation, *Volume I*, C. Vigo-Pelfrey, ed. (Boston: CRC Press), pp. 239–268.

Esterbauer, H., Schaur, R.J., and Zollner, H. (1991). Chemistry and biochemistry of 4-hydroxynonenal, malonaldehyde and related aldehydes. Free Radic. Biol. Med. *11*, 81–128.

Ferrone, F. (1999). Analysis of protein aggregation kinetics. Methods Enzymol. *309*, 256–274.

Hernandez-Boussard, T., Rodriguez-Tome, P., Montesano, R., and Hainaut, P. (1999). IARC p53 mutation database; a relational database to compile and analyze p53 mutations in human tumors and cell lines. International Agency for Research on Cancer. Hum. Mutat. *14*, 1–8.

Hollstein, M., Sidransky, D., Vogelstein, B., and Harris, C. (1991). p53 mutations in human cancers. Science *253*, 49–53.

Hurshman, A.R., White, J.T., Powers, E.T., and Kelly, J.W. (2004). Transthyretin aggregation under partially denaturing conditions is a downhill polymerization. Biochemistry *43*, 7365–7381.

Isaacs, J.S., Hardman, R., Carman, T.A., Barrett, J.C., and Weissman, B.E. (1998). Differential subcellular p53 localization and function in N- and S-type neuroblastoma cell lines. Cell Growth Differ. *9*, 545–555.

Kastan, M.B., Onyekwere, O., Sidransky, D., Vogelstein, B., and Craig, R.W. (1991). Participation of p53 protein in the cellular response to DNA damage. Cancer Res. *51*, 6304–6311.

Keeley, D., and Rees, J. (1997). New guidelines in asthma management. BMJ *314*, 315–316.

Kelly, J.W. (1998). The alternative conformations of amyloidogenic proteins and their multi-step assembly pathways. Curr. Opin. Struct. Biol. *8*, 101–106.

Lane, D.P. (1992). p53, guardian of the genome. Nature *358*, 15–16.

Levine, A.J., Momand, J., and Finlay, C.A. (1991). The p53 tumour suppressor gene. Nature *351*, 453–456.

LeVine, H., III. (1999). Quantification of [beta]-sheet amyloid fibril structures with thioflavin T. Methods Enzymol. *309*, 274–284.

Lu, H., Ouyang, W., and Huang, C. (2006). Inflammation, a key event in cancer development. Mol. Cancer Res. *4*, 221–233.

Moll, U.M., Riou, G., and Levine, A.J. (1992). Two distinct mechanisms alter p53 in breast cancer: mutation and nuclear exclusion. Proc. Natl. Acad. Sci. USA *89*, 7262–7266.

Moll, U.M., LaQuaglia, M., Benard, J., and Riou, G. (1995). Wild-type p53 protein undergoes cytoplasmic sequestration in undifferentiated neuroblastomas but not differentiated tumors. Proc. Natl. Acad. Sci. USA *92*, 4407–4411.

Moos, P.J., Edes, K., and Fitzpatrick, F.A. (2000). Inactivation of wild-type p53 tumor suppressor by electrophilic prostaglandins. Proc. Natl. Acad. Sci. USA *97*, 9215–9220.

Moos, P.J., Edes, K., Cassidy, P., Massuda, E., and Fitzpatrick, F.A. (2003). Electrophilic prostaglandins and lipid aldehydes repress redox-sensitive transcription factors p53 and hypoxia-inducible factor by impairing the selenoprotein thioredoxin reductase. J. Biol. Chem. *278*, 745–750.

Nieva, J., Shafton, A., Altobell, L.J., Tripuraneni, S., Rogel, J.K., Wentworth, A.D., Lerner, R.A., and Wentworth, P. (2008). Lipid-derived aldehydes accelerate light chain amyloid and amorphous aggregation. Biochemistry *47*, 7695–7705.

Philip, M., Rowley, D.A., and Schreiber, H. (2004). Inflammation as a tumor promoter in cancer induction. Semin. Cancer Biol. *14*, 433–439.

Scheinost, J.C., Wang, H., Boldt, G.E., Offer, J., and Wentworth, P.J., Jr. (2008). Cholesterol seco-sterol-induced aggregation of methylated amyloid-β peptides—insights into aldehyde-initiated fibrillization of amyloid-β. Angew. Chem. Int. Ed. Engl. *47*, 3919–3922.

Scheinost, J.C., Witter, D.P., Boldt, G.E., Offer, J., and Wentworth, P.J., Jr. (2009). Cholesterol secosterol adduction inhibits the misfolding of a mutant prion protein fragment that induces neurodegeneration. Angew. Chem. Int. Ed. Engl. *48*, 9469–9472.

Takeuchi, C., Galve, R., Nieva, J., Witter, D.P., Wentworth, A.D., Troseth, R.P., Lerner, R.A., and Wentworth, P., Jr. (2006). Proatherogenic effects of the cholesterol ozonolysis products, atheronal-A and atheronal-B. Biochemistry *45*, 7162–7170.

Tominaga, O., Hamelin, R., Trouvat, V., Salmon, R.J., Lesec, G., Thomas, G., and Remvikos, Y. (1993). Frequently elevated content of immunochemically defined wild-type p53 protein in colorectal adenomas. Oncogene *8*, 2653–2658.

Uversky, V.N., and Fink, A.L. (2004). Conformational constraints for amyloid fibrillization: the importance of being unfolded. Biochim. Biophys. Acta *1698*, 131–153.

Vogelstein, B., and Kinzler, K.W. (1992). p53 function and dysfunction. Cell *70*, 523–526.

Wentworth, P., Jr., Nieva, J., Takeuchi, C., Galve, R., Wentworth, A.D., Dilley, R.B., DeLaria, G.A., Saven, A., Babior, B.M., Janda, K.D., et al. (2003). Evidence for ozone formation in human atherosclerotic arteries. Science *302*, 1053–1056.

Zambetti, G.P., and Levine, A.J. (1993). A comparison of the biological activities of wild-type and mutant p53. FASEB J. *7*, 855–865.

Zhang, Q., Powers, E.T., Nieva, J., Huff, M.E., Dendle, M.A., Bieschke, J., Glabe, C.G., Eschenmoser, A., Wentworth, P., Jr., Lerner, R.A., and Kelly, J.W. (2004). Metabolite-initiated protein misfolding may trigger Alzheimer's disease. Proc. Natl. Acad. Sci. USA *101*, 4752–4757.